Broadband signal response of thermo-acoustic devices and its applications

L. H. Tong,[1,a)] S. K. Lai,[2] and C. W. Lim[3]
[1]*School of Civil Engineering and Architecture, East China Jiaotong University, Nanchang, Jiangxi, People's Republic of China*
[2]*Department of Civil and Environmental Engineering, The Hong Kong Polytechnic University, Hung Hom, Kowloon, Hong Kong, People's Republic of China*
[3]*Department of Architecture and Civil Engineering, City University of Hong Kong, Kowloon, Hong Kong SAR, People's Republic of China*

(Received 5 January 2017; revised 18 March 2017; accepted 20 March 2017; published online 6 April 2017)

Thermo-acoustic (TA) transducers are generation of sound speakers without any mechanical vibration system which exhibit an extremely wide frequency response range. In this paper, acoustic field responses to broadband input signals applied to both free-standing and nano-thinfilm-substrate thermo-acoustic devices are developed theoretically by using the Fourier transformation. A series of signals, including single-frequency signal, square root signal, periodic triangle wave signal, and periodic rectangular pulse signal, are applied to these TA devices in simulations and the acoustic pressure responses are investigated. The reproducibility of input signals is predicted. The single frequency results show good agreement with previously published experimental results. Alternative methods for reproducing the original signals with small distortion and low power consumption are introduced. The excellent performance of the TA devices on broadband signal responses will provide a design approach for sound parametric array and underwater communication equipment.
 [http://dx.doi.org/10.1121/1.4979667]

[MRB] Pages: 2430–2439

I. INTRODUCTION

Thermo-acoustic (TA) devices exhibit an entirely different acoustic generation mechanism comparing with the conventional mechanically driven audio frequency devices or ultrasound transducers. There is no mechanical movement of the devices involved in sound generation, and thus no resonance peaks are produced. As a result, a wide frequency range of sound can be efficiently generated. When an alternating current signal is applied to a TA device, the surrounding medium (gas or fluid) is heated periodically. An oscillating temperature field for the medium is induced and it results in expansion and contraction of the medium that generates acoustic waves (Venkatasubramanian, 2010). Taking advantage of the TA device, new audio frequency devices can be devised to bring alternative form factors and a breakthrough technology in designing high-power sonar array for underwater communication. With the rapid development of nanotechnology, thermo-acoustic sound generation using nano-thinfilms (NTFs) has attracted much research interests in recent years, although the concept of thermo-phone was already introduced almost a century ago (Arnold and Crandall, 1917). The first efficient TA device was designed and characterized by Shinoda *et al.* (Shinoda *et al.*, 1999). In the device, a 30 nm thick aluminum film was placed on a micro-porous silicon layer to serve as a major element for sound generation. Comparing with conventional mechanically driven sound generation devices, more energy was necessary to obtain the same sound pressure level by using aluminum NTFs sound device. It is because most of the thermal energy generated by the NTFs leaked into the substrate. Nevertheless, the distinct advantage of the TA device is its wide effective broadband frequency response range that is unachievable by the mechanically driven devices. This broadband frequency characteristic has been proved to have tremendously simplified the design of a sound speaker (Wei *et al.*, 2013). Based on experiments (Xiao *et al.*, 2008; Xiao *et al.*, 2011) and theoretical studies (Lim *et al.*, 2013; Tong *et al.*, 2013), it was demonstrated that for a TA sound source to be practically efficient, it required a small heat capacity per unit area (HCPUA). To further improve the performance of a TA device, the use of carbon nanotube sheets (CNT) (Xiao *et al.*, 2008) was reported to be capable of emitting powerful sound pressure waves in air.

Subsequently, other kinds of TA devices were reported, including devices manufactured by CNT assemblies (Kozlov *et al.*, 2009), metallic wires array and thin-metallic layer (Niskanen *et al.*, 2009; Vesterinen *et al.*, 2010; Tian *et al.*, 2011b; Chitnis *et al.*, 2012; Koshida *et al.*, 2013), graphene films (Tian *et al.*, 2011a; Suk *et al.*, 2012; Tian *et al.*, 2012; Tian *et al.*, 2014), suspended CNT-yarn array on a substrate (Wei *et al.*, 2013), individual suspended CNT (Mason *et al.*, 2015) and carbonized nano-fiber sheets (Aliev *et al.*, 2016). The performance of TA devices immersed in various environments was also investigated. The thermo-acoustic sound pressure responses in several fluidic media, such as ethanol, methanol and water was studied (Aliev *et al.*, 2010) to indicate that the pressure generation efficiency in water was a

[a)]Electronic mail: lhtong@ecjtu.edu.cn

hundred-fold over that in wetting alcohol due to the hydrophobicity of the nanotube sheets in water. Besides, the sound response characteristics of TA devices in different gaseous media were also investigated in open space (Xiao *et al.*, 2011) and in closed systems (Aliev *et al.*, 2013) over a wide frequency range. It was revealed that the pressure responses in open and closed systems were completely different. In addition, the thermal properties of gaseous medium have significant influence on sound generation. However, the unavailability of large-size, free-standing CNT sheets for practical devices (Aliev *et al.*, 2015) and the low energy conversion efficient of graphene-based TA devices due to thermal leakage jeopardize the technological development of thermo-acoustic applications. In order to overcome the structure weakness of a free-standing CNT film, a well-designed TA chip with a robust structure by suspending the CNT thin yarn array on a patterned silicon wafer was proposed (Wei *et al.*, 2013). To prevent thermal leakage into the substrate, laser-scribed graphene (LSG) technique was developed. The presence of air gaps between the graphene layers was beneficial for the emission of thermo-acoustic wave (Tian *et al.*, 2014). Theoretically, it was also demonstrated that the air gap that separated the NTF and substrate could enhance energy conversion (Tong *et al.*, 2015). Some alternative nanostructures for manufacturing high energy-conversion efficiency, environmentally and cost-effective TA devices were also proposed (Aliev *et al.*, 2015).

Although intensive experiment studies on thermo-acoustics were reported, few works on theoretical investigations were attempted. For theoretical analysis, a fully coupled thermal-mechanical equation was solved to analyze the ultrasound pressure field generated by an aluminum NTF placed on a porous silicon substrate (Hu *et al.*, 2010). Xiao *et al.* (Xiao *et al.*, 2008) introduced a new key factor HCPUA to improve the model proposed by Arnold and Crandall (Arnold and Crandall, 1917) for explaining the experimental observation. Vesterinen *et al.* (Vesterinen *et al.*, 2010) investigated the efficiency of TA devices and the thermal leakage effect on sound generation. In an attempt to explain the experiment results (Xiao *et al.*, 2008; Xiao *et al.*, 2011), Lim *et al.* (Lim *et al.*, 2013) proposed an accurate analytical solution for free-standing NTFs, a good agreement to experimental observation was reported. Subsequently, Tong and his associates (Tong *et al.*, 2013; Tong *et al.*, 2015) studied two specific TA structures, i.e., the gas-filled encapsulated TA transducer and gap-separation TA device. The proposed analytical models were verified by some published experiment results. More recently, a cylindrical TA model was also presented (Tong *et al.*, 2016) to investigate an individual CNT thermo-acoustic response. With respect to the aforementioned works on TA sound generation, it is found that all experiment and theoretical works only focus on single-frequency TA pressure responses. Under most circumstances, a TA device can undertake multi-frequency input signals on the premise of low distortion. However, to the best knowledge of the authors, there have been no attempts in this respect.

In this paper, new and significant TA sound generation for broadband input signals is developed. Theoretical solutions are obtained by applying the Fourier transformation and its inverse. Highly accurate and approximate sound pressure expressions are derived and reported. Some specific input signal forms, including rectangular pulse signal, triangle signal and square root signal, are employed for investigating the corresponding sound pressure responses. It is concluded that for a signal with frequency spectrum that concentrates within a certain frequency range, the acoustic signal output is able to reproduce the input signal form. From a practical point of view, new and alternative design methods for recovering the original signals for TA sound responses are introduced.

II. ANALYTICAL MODELLING AND SOLUTION METHODOLOGY

A TA sound wave can be generated by introducing an alternating current to a TA device. There are two kinds of TA devices that are frequently used. The first is a free-standing nano-thinfilm TA device and the second one is a nano-thinfilm-substrate (NTF-substrate). There are no essential differences in TA sound generation mechanism for these two kinds of devices. However, the energy conversion efficiency for these two devices is different. The TA sound waveform generated by an input broadband frequency signal will be analyzed with respect to these devices. The problem studied here is indeed a thermal-mechanical coupled system. For the sake of clarity and convenience, the thermal and acoustic fields are presented separately in the subsequent sections.

A. Thermal field

The coupled temperature field equation within the context of linear and non-viscous conditions is (Vesterinen *et al.*, 2010; Beranek and Mellow, 2012)

$$\nabla^2 T - \frac{1}{\alpha}\frac{\partial T}{\partial t} = -\frac{1}{\kappa}\frac{\partial p}{\partial t}, \tag{1}$$

where T is the varying temperature field, α is the thermal diffusivity of medium, κ is the heat conductivity of medium, p is the acoustic pressure, and t is time. For a free-standing TA device, the thermal energy transfers to the surrounding gaseous medium from both sides of the NTF. In contrast, for a NTF-substrate TA device, the thermal energy transfers to the surrounding gaseous medium on one side and to the substrate on the other side. Therefore, the thermal fields generated by these two kinds of devices are different.

1. Free-standing TA device

The schematic of a free-standing TA device is shown in Fig. 1. When a signal $A_0 f(t)$ with an arbitrary wave form (not limited to a harmonic wave) and the amplitude A_0 with unit ampere is applied to the device, a corresponding thermal field is generated. As the contribution of acoustic pressure variation to the temperature field is significantly small, the term $-\partial_t p/\kappa$ in Eq. (1) can be neglected. Hence, the thermal field equation in the gaseous medium is further simplified as

$$\nabla^2 T_g - \frac{1}{\alpha_g}\frac{\partial T_g}{\partial t} = 0, \tag{2}$$

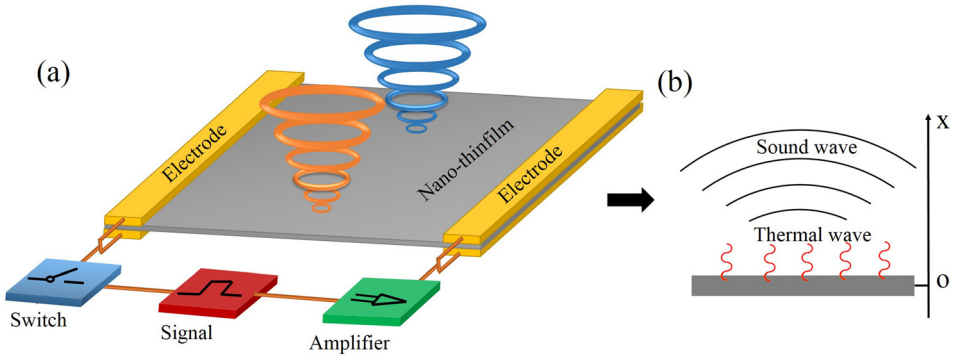

FIG. 1. (Color online) (a) A thermo-acoustic device fabricated by suspending a nano-thinfilm in a gaseous medium and (b) the coordinate arrangement. The switch block is responsible for controlling the circuit on and off. The amplifier block is employed to amplify the input signal which is generated by the signal block.

where subscript g stands for variables related to a gaseous medium.

In the near-field, the temperature wave is a plane wave. Because the input signal contains a broadband frequency range, assuming time-dependent "$e^{j\omega t}$" to reduce the governing equation from initially a partial differential equation to an ordinary differential equation is not fully valid. Applying Fourier transformation to the thermal field $T_g(x,t)$ to convert the thermal field from time domain to frequency domain yields

$$\mathcal{F}[T_g(x,t)] = \frac{1}{\sqrt{2\pi}}\int_{-\infty}^{+\infty} T_g(x,t)e^{-j\omega t}dt = \bar{T}_g(x,\omega), \quad (3)$$

then Eq. (2) is transformed to

$$\frac{d^2\bar{T}_g}{dx^2} - \frac{j\omega}{\alpha_g}\bar{T}_g = 0. \quad (4)$$

The thickness of NTF at typically the order of nanometers is considered. For a film that is located at $x = 0$, obviously, the thermal field is symmetric for $x > 0$ and for $x < 0$. Thus only the thermal field for $x > 0$ is considered here. Because $\bar{T}_g(x,\omega)$ is finite when $x \to \infty$, the solution of Eq. (4) is obtained as

$$\bar{T}_g(x,\omega) = C_{g1}(\omega)e^{j\lambda_g x} \quad (x > 0), \quad (5)$$

where $\lambda_g = -\sqrt{\omega/(2\alpha_g)} + j\sqrt{\omega/(2\alpha_g)}$. To determine $C_{g1}(\omega)$, the thermal balance equation (Tong *et al.*, 2015; Tong *et al.*, 2016) is considered and it is expressed as

$$RA_0{}^2 g(t) = 2s\beta_0 T_f(t) + sQ_- + sQ_+ + sc_s\frac{dT_f(t)}{dt}, \quad (6)$$

where R, s, $T_f(t)$, and c_s are the electrical resistance, area, time-dependent temperature and unit area heat capacity of NTF, respectively, β_0 is the rate of heat loss per unit area, $Q_\pm = \mp\kappa_g \partial T_g(x,t)/\partial x|_{x=0^\pm}$ are the instantaneous heat exchange per unit area between NTF and its surrounding medium in front and back of NTF, and $g(t) = f^2(t)$. Applying Fourier transformation on Eq. (6), substituting Eq. (5) into Eq. (6) and assuming $\bar{T}_f(\omega) = \bar{T}_g(0,\omega)$, $C_{g1}(\omega)$ is then determined as

$$C_{g1}(\omega) = \bar{T}_f(\omega) = \frac{RA_0{}^2 G(\omega)}{2s\beta_0 - j2s\lambda_g\kappa_g - js\omega c_s}, \quad (7)$$

where $G(\omega) = \mathcal{F}[g(t)]$. Equations (5) and (7) present the thermal field in a frequency domain. Applying inverse Fourier transformation on Eq. (5) yields the solution in a time domain. Since the ultimate goal is to derive the solution of the acoustic pressure field, the thermal field solution in a frequency domain will be further used to determine the acoustic pressure field. Hence, the thermal field solution in the time domain is not presented here.

2. NTF-substrate TA device

The schematic of a NTF-substrate TA device is shown in Fig. 2. In this case, the thermal property of the substrate has significant influence on the thermal field of the surrounding gaseous medium. It is similar to the model and analysis aforementioned. Contribution of the variation of acoustic pressure on the thermal field can be neglected, and the thermal field equation reads

$$\nabla^2 T_i - \frac{1}{\alpha_i}\frac{\partial T_i}{\partial t} = 0, \quad (i = g, s), \quad (8)$$

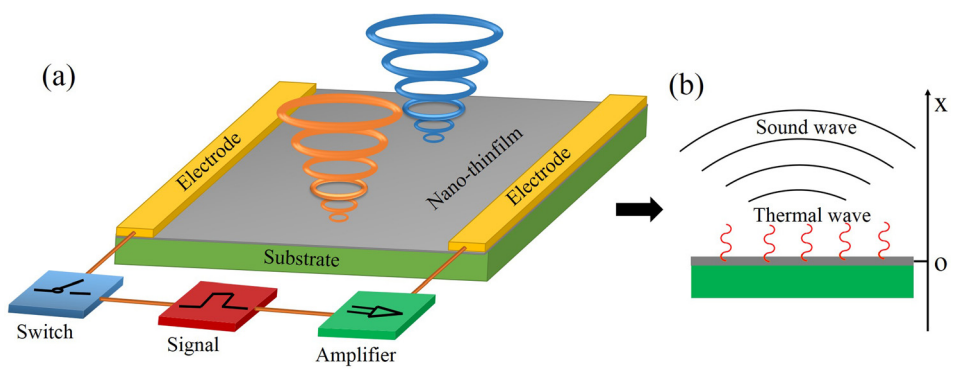

FIG. 2. (Color online) (a) A NTF-substrate TA device fabricated by locating a nano-thinfilm directly on a substrate and (b) the coordinate arrangement. The functions of switch block, amplifier block and signal block is elaborated in the caption to Fig. 1.

where the subscripts g and s stand for the variables related to the gaseous medium and the substrate, respectively.

Applying Fourier transformation on Eq. (8) yields

$$\frac{d^2\bar{T}_i}{dx^2} - \frac{j\omega}{\alpha_i}\bar{T}_i = 0. \tag{9}$$

It is assumed that the substrate thickness is sufficiently large and the thermal wave in the substrate is attenuated before arriving at the back. Here the film is also located at $x = 0$. The solutions for the gaseous medium and the substrate can be obtained as

$$\begin{aligned} \bar{T}_g(x,\omega) &= C_{g2}(\omega)e^{j\lambda_g x} \quad (x > 0), \\ \bar{T}_s(x,\omega) &= C_s(\omega)e^{-j\lambda_s x} \quad (x < 0), \end{aligned} \tag{10}$$

where $\lambda_s = -\sqrt{\omega/(2\alpha_s)} + j\sqrt{\omega/(2\alpha_s)}$ and λ_g is defined in Eq. (5) above. The boundary conditions at $x = 0$ is $\bar{T}_g(0,\omega) = \bar{T}_s(0,\omega) = \bar{T}_f(\omega)$. Taking advantage of the thermal balance Eq. (6) and the boundary conditions, and noting that $Q_+ = -\kappa_g[d\bar{T}_g/dx]|_{x=0^+}$ and $Q_- = \kappa_s[d\bar{T}_s/dx]|_{x=0^-}$, the coefficients $C_s(\omega)$ and $C_{g2}(\omega)$ are determined as

$$\begin{aligned} C_{g2}(\omega) &= C_s(\omega) = \bar{T}_f(\omega), \\ \bar{T}_f(\omega) &= \frac{RA_0{}^2G(\omega)}{2s\beta_0 - js\lambda_g\kappa_g - js\lambda_s\kappa_s - js\omega c_s}. \end{aligned} \tag{11}$$

The thermal fields in a frequency domain for both gaseous medium and substrate are given by Eqs. (10) and (11). The thermal field of gaseous medium is of great interest to us, so the thermal field of substrate will not be further studied. Similarly, the thermal field expressed in terms of a frequency domain will be further used to determine the acoustic field, thus the time-domain solution is not presented here although it can be obtained by the inverse Fourier transformation.

B. Acoustic field

The coupled isentropic acoustic wave equation in the surrounding medium is (Tong *et al.*, 2015)

$$\nabla^2 P - \frac{1}{C_0{}^2}\frac{\partial^2 P}{\partial t^2} = -\alpha_g\frac{\rho_0}{T_0}\frac{\partial(\nabla^2 T_g)}{\partial t}, \tag{12}$$

where P is the acoustic pressure, ρ_0 is the density of surrounding medium, T_0 is the temperature of ambient surrounding medium and C_0 is the isentropic speed of sound. Applying Fourier transformation on Eq. (12) and using Eq. (5) or Eq. (10) yield

$$\frac{\mathrm{d}^2\bar{P}(x,\omega)}{\mathrm{d}x^2} + k^2\bar{P}(x,\omega) = \omega^2\frac{\rho_0}{T_0}C_{gi}(\omega)e^{j\lambda_g x} \quad (i = 1,2), \tag{13}$$

where $k = \omega/C_0$, $i = 1$ and $i = 2$ correspond to the acoustic field generated by the free-standing TA device and the NTF-substrate TA device, respectively.

Consider an infinite space (i.e., no reflecting wave field), the homogeneous solution to Eq. (13) is

$$\bar{P}_{hi}(x,\omega) = D_i(\omega)e^{-jkx}(i = 1,2), \tag{14}$$

where $D_i(\omega)$ is an undetermined coefficient. The particular solution to Eq. (13) is

$$\bar{P}_{si}(x,\omega) = \omega^2\frac{\rho_0}{T_0}\frac{1}{k^2 - \lambda_g{}^2}C_{gi}(\omega)e^{j\lambda_g x} \quad (i = 1,2). \tag{15}$$

The solution to Eq. (13) can be obtained as

$$\bar{P}_i(x,\omega) = \bar{P}_{hi}(x,\omega) + \bar{P}_{si}(x,\omega) \quad (i = 1,2). \tag{16}$$

As the NTF can be treated as an infinite impedance plane, $D_i(\omega)$ in Eq. (14) can be determined by using the boundary condition at $x = 0$, i.e., $[d\bar{P}(x,\omega)/dx]|_{x=0} = 0$, as

$$D_i(\omega) = \frac{\rho_0}{T_0}\frac{\omega^2}{k}\frac{\lambda_g}{k^2 - \lambda_g{}^2}C_{gi}(\omega). \tag{17}$$

Consider full attenuation of the particular solution, the acoustic field can be further simplified as

$$\bar{P}_i(x,\omega) = \frac{\rho_0 C_0}{T_0}\frac{\lambda_g\omega}{k^2 - \lambda_g{}^2}C_{gi}(\omega)e^{-jkx} \quad (i = 1,2). \tag{18}$$

Applying inverse Fourier transformation on Eq. (18), the acoustic field in a time domain can be obtained as

$$P_i(x,t) = \frac{1}{\sqrt{2\pi}}\int_{-\infty}^{+\infty}\bar{P}_i(x,\omega)e^{j\omega t}d\omega \quad (i = 1,2). \tag{19}$$

The integral in Eq. (19) is complex and it is difficult to obtain an explicit expression for an arbitrary input signal $G(\omega)$. In view of this problem, some restrictive conditions are assumed and explicit analytical acoustic field solutions can be obtained subject to these conditions.

C. Simplification of acoustic field integration

The acoustic field in Eq. (19) can be easily solved if the input signal is governed by a single circular frequency ω_0. Equivalently, when $G(\omega) = \sqrt{2\pi}\delta(\omega - \omega_0)$, the acoustic field can be obtained as

$$P_i(x,t) = \bar{P}_i(x,\omega_0)e^{j\omega_0 t} \quad (i = 1,2). \tag{20}$$

However, in most circumstances, the input signal possesses a wide frequency spectrum and the integral in Eq. (19) is complex. Here, some restrictive conditions on the frequency are assumed in order to simplify the integration.

(1) For $\omega \ll C_0{}^2/\alpha_g$, we have $|\lambda^2| \gg |k^2|$, then

$$\frac{\omega}{(k^2 - \lambda_g{}^2)} \approx -j\alpha_g. \tag{21}$$

(2) For $(\alpha_g\beta_0{}^2)/\kappa_g{}^2 \ll \omega \ll (4\kappa_g{}^2)/(\alpha_g c_s{}^2)$, we have $|j2\lambda_g\kappa_g| \gg 2\beta_0$ and $|j2\lambda_g\kappa_g| \gg |j\omega c_s|$, then

$$\frac{\lambda_g}{(2\beta_0 - j2\lambda_g\kappa_g - j\omega c_s)} \approx \frac{j}{(2\kappa_g)}. \quad (22)$$

(3) For $(4\alpha_i\beta_0{}^2)/\kappa_i{}^2 \ll \omega \ll (\kappa_i{}^2)/(\alpha_i c_s{}^2)$ $(i = g, s)$, we have $|j\lambda_i\kappa_i| \gg 2\beta_0$ and $|j\lambda_i\kappa_i| \gg |j\omega c_s|$, then

$$\frac{\lambda_g}{(2\beta_0 - j\lambda_s\kappa_s - j\lambda_g\kappa_g - j\omega c_s)} \approx \frac{j\sqrt{\alpha_g}}{\kappa_g\sqrt{\alpha_s} + \kappa_s\sqrt{\alpha_g}}. \quad (23)$$

Synthesizing the conditions (1) and (2) above, the acoustic pressure for the free-standing TA device in a frequency domain can be further simplified as

$$\bar{P}_1(x,\omega) = P_{in}\frac{\gamma-1}{2C_0}G(\omega)e^{-jkx}$$
$$\text{Condition}: (\alpha_g\beta_0{}^2)/\kappa_g{}^2 \ll \omega \ll \text{Min}\{(4\kappa_g{}^2)/(\alpha_g c_s{}^2), C_0{}^2/\alpha_g\}. \quad (24)$$

Similarly, by making use of the conditions (1) and (3), the acoustic pressure for the NTF-substrate TA device in a frequency domain can be further simplified as

$$\bar{P}_2(x,\omega) = P_{in}\frac{\gamma-1}{2C_0}RG(\omega)e^{-jkx}$$
$$\text{Condition}: \text{Max}\{4(\alpha_i\beta_0{}^2)/\kappa_i{}^2\} \ll \omega \ll \text{Min} \times \{(\kappa_i{}^2)/(\alpha_i c_s{}^2), C_0{}^2/\alpha_g\}, i = g, s, \quad (25)$$

where $\mathcal{R} = 2\sqrt{\alpha_g}/(\kappa_g\sqrt{\alpha_s} + \kappa_s\sqrt{\alpha_g})$, $P_{in} = RA_0{}^2/s$, γ the specific heat ratio of gas. It should be noted that relations $\sqrt{\gamma P_0/\rho_0} = C_0$ and $(\gamma-1)T_0/(\gamma P_0) = \alpha_g/\kappa_g$ are used to obtain Eqs. (24) and (25).

If air is assumed as the surrounding gaseous medium and a single-layer CNT sheet is modelled as the NTF [$c_s = 7.7 \times 10^{-3}\text{Jm}^{-2}\text{K}^{-1}$, $\beta_0 = 23\text{WK}^{-1}\text{m}^{-2}$ (Xiao *et al.*, 2008)], then by substituting the relevant parameter values of air and NTF into condition Eq. (24), we have $17.3\,\text{rad/s} \ll \omega \ll 2 \times 10^6\text{rad/s}$ (i.e., 2.75 Hz $\ll f \ll$ 0.32 MHz). It is obvious that the approximate acoustic field expressed in Eq. (24) stands for a wide frequency range. It is easy to draw a similar conclusion by numerical analysis for the condition in Eq. (25). Therefore, if the frequency spectrum of an input signal mainly concentrates in this frequency range, the acoustic field in a time domain can be obtained by substituting the approximate expression in Eq. (24) or Eq. (25) to the integration in Eq. (19) as

$$P_i(x,t) \approx \frac{1}{\sqrt{2\pi}}\int_{-\infty}^{+\infty} P_{in}\frac{\gamma-1}{2C_0}\mathcal{R}_i G(\omega)e^{-jkx}e^{j\omega t}d\omega = P_{in}\frac{\gamma-1}{2C_0}\mathcal{R}_i \cdot g\left(t - \frac{x}{C_0}\right) \quad (i = 1, 2), \quad (26)$$

where $\mathcal{R}_1 = 1$ for the free-standing TA device and $\mathcal{R}_2 = \mathcal{R}$ for the NTF-substrate TA device. From Eq. (26), the output acoustic pressure signal has a similar form to that of the original signal $g(t)$. Therefore, signal $g(t)$ can be generated by the TA device with the acoustic wave propagating away with a small distortion if the frequency spectrum of $g(t)$ concentrates within the frequency range prescribed by the conditions in Eqs. (24) and (25).

The acoustic fields expressed in Eqs. (19) or (26) are only suitable for the near field. For a single-frequency response, the acoustic field on the central axis in the far field can be easily obtained by multiplying R_0/x to Eq. (20) with $R_0 = s\omega_0/(2\pi C_0)$ as

$$P_i(x,t) = \frac{R_0}{x}\bar{P}_i(x,\omega_0)e^{j\omega_0 t} \quad (i = 1, 2). \quad (27)$$

When the input signal is a broadband signal, the acoustic pressure in the far field can be obtained from the near field solution. This is the scope of further investigation.

III. PRACTICAL CASES OF STUDY

A. Single-frequency signal $g(t) = \text{Exp}(j\omega_0 t)$

For the first case, a single-frequency input signal $g(t) = e^{j\omega_0 t}$ is chosen to verify the analytical model. The NTF is chosen as a single-layer CNT sheet with a HCPUA $c_s = 7.7 \times 10^{-3}\text{Jm}^{-2}\text{K}^{-1}$ and area $3 \times 3\,\text{cm}^2$, as indicated by Xiao *et al.* (Xiao *et al.*, 2008). The TA device is located in air at normal temperature and atmospheric pressure and the thermal properties of air are shown in Table I. The relevant parameters of air similar to Xiao *et al.* (Xiao *et al.*, 2008) are adopted. Exact theoretical predictions and approximate solutions are compared with experiment results (Xiao *et al.*, 2008) as shown in Fig. 3(a). It is clear that the approximate solution in Eq. (24) is in good agreement with the exact solution in Eq. (20). A good consistency between the experiment and theoretical results also verifies the new analytical model developed here. It should be emphasized that the theoretical results presented in Fig. 3 are not directly calculated by using Eqs. (20) and (24) because the observation point ($x = 5\,\text{cm}$) is beyond the near field range. Therefore, the far field acoustic pressure expression is used for theoretical prediction.

To verify the analytical model of the NTF-substrate TA device, the acoustic pressure response for a single-frequency input signal $g(t) = e^{j\omega_0 t}$ is investigated. Shinoda *et al.* (Shinoda *et al.*, 1999) proposed an experiment for a TA device by placing a thin aluminum film on a porous silicon substrate and the thermal properties of porous silicon are shown in Table I. The experimental observation is compared with theoretical results predicted by the new analytical model developed here for both the far and near fields as shown in Fig. 3(b). Obviously, good agreement is demonstrated between experiment and theoretical results. The thermal properties of the substrate by Shinoda *et al.* (Shinoda *et al.*, 1999) are adopted and the observation point is located at $x = 3.5\,\text{cm}$. Furthermore, the approximate solution coincides

TABLE I. Thermal properties of air and porous silicon at 300 K.

	α (mm^2s^{-1})	κ ($\text{W m}^{-1}\text{K}^{-1}$)	ρC_P ($\text{J m}^{-3}\text{K}^{-1}$)
Air (Aliev *et al.*, 2013)	21.7	0.0259	1191.1
Porous silicon (Shinoda *et al.*, 1999)	1.43	1	0.7×10^6

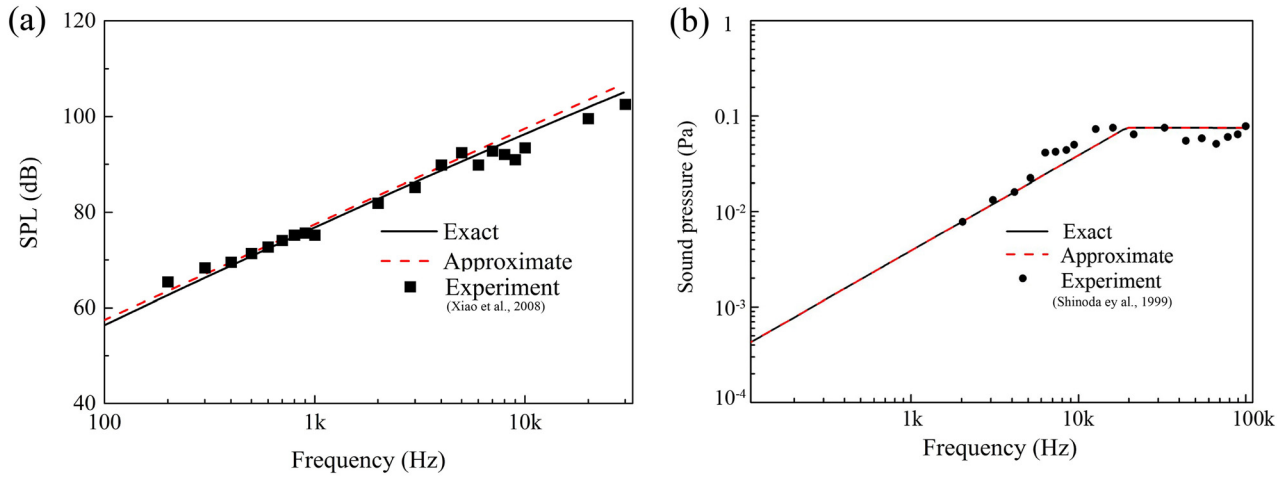

FIG. 3. (Color online) (a) Comparison of exact and approximate predictions with experiment for a free-standing TA device fabricated by a $3 \times 3\,\mathrm{cm}^2$ CNT sheet. The input power is 4.5 W and the observation point is at $x = 5$ cm on the central axis. (b) Comparison of exact and approximate predictions with experiment for a NTF-substrate TA device fabricated by a $2.5 \times 2.5\,\mathrm{cm}^2$ aluminum film with HCPUA $c_s = 7.2 \times 10^{-2}\mathrm{Jm}^{-2}\mathrm{K}^{-1}$ and a porous silicon substrate. The input power is $1\,\mathrm{W/cm}^2$ and the observation point is at $x = 3.5$ cm cm on the central axis.

closely with the exact solution and it confirms the validity of the approximate solution.

B. Square root signal $g(t) = \sqrt{1+\cos(\omega_0 t)}$

The analytical model proposed here has been verified earlier by comparing with experiment for both the NTF-substrate and free-standing TA devices. From this section onwards, we limit the investigation on the free-standing TA device fabricated by a single-layer CNT sheet. The surrounding medium is taken as air. From Eq. (26), the approximate solution for acoustic pressure can be directly expressed as

$$P_1(x,t) \approx P_{in}\frac{\gamma-1}{2C_0}\cdot\sqrt{1+\cos\left(\omega_0 t-\frac{\omega_0 x}{C_0}\right)}. \tag{28}$$

As $g(t)$ is a broadband signal, an explicit analytical expression for the integral in Eq. (19) is difficult. For this reason, $g(t)$ is transformed into a cosine series as follows

$$g(t) = \frac{2\sqrt{2}}{\pi} + \sum_{n=1}^{\infty}\frac{(-1)^{n-1}4\sqrt{2}}{(4n^2-1)\pi}\cos(n\omega_0 t). \tag{29}$$

Applying Fourier transformation on Eq. (29) yields

$$G(\omega) = \frac{4}{\sqrt{\pi}}\delta(\omega) + \sum_{n=1}^{\infty}\sqrt{\frac{\pi}{2}}\frac{(-1)^{n-1}4\sqrt{2}}{(4n^2-1)\pi} \times \left[\delta(\omega-n\omega_0)+\delta(\omega+n\omega_0)\right]. \tag{30}$$

Substituting Eq. (30) into Eq. (19), the integral can be solved and the acoustic pressure is obtained as

$$P_1(x,t) = \frac{2\sqrt{2}}{\pi}\bar{P}_1(x,0) + \sum_{n=1}^{\infty}\frac{(-1)^{n-1}2\sqrt{2}}{(4n^2-1)\pi} \times \left[\bar{P}_1(x,n\omega_0)e^{jn\omega_0 t}+\bar{P}_1(x,-n\omega_0)e^{-jn\omega_0 t}\right]. \tag{31}$$

It is found that the acoustic pressure is the summation of a set of infinite series but the series can be verified to be fast convergent. For $\omega_0 = 0$, it implies $\bar{P}_1(x,0) = 0$ and thus the first term in $P_1(x,t)$ disappears. Equivalently, the direct-current (DC) component does not contribute to any acoustic pressure effect. However, from Eq. (28), the DC component does exist and it contributes to the acoustic pressure which leads to inconsistent results. It is because the approximate solution of Eq. (28) is obtained by assuming $\omega \gg 17.3\,\mathrm{rad/s}$. For non-negligible DC component of the input signal, the approximate solution in Eq. (26) should be corrected as

$$P_i(x,t) \approx P_{in}\frac{\gamma-1}{2C_0}\mathcal{R}_i\cdot\left[g\left(t-\frac{x}{C_0}\right)-\mathrm{g(DC)}\right] \quad (i=1,2), \tag{32}$$

where $g(\mathrm{DC})$ is the DC component of the signal $g(t)$, for example, $g(\mathrm{DC}) = 2\sqrt{2}/\pi$ is selected. Consequently, the approximate solution for this case can be obtained as

$$P_1(x,t) \approx P_{\mathrm{in}}\frac{\gamma-1}{2C_0}\left[g\left(t-\frac{x}{C_0}\right)-\frac{2\sqrt{2}}{\pi}\right]. \tag{33}$$

For a $3 \times 3\,\mathrm{cm}^2$ CNT sheet NTF, the acoustic fields predicted by Eqs. (31) and (33) at $\omega_0 = 2000\,\mathrm{rad/s}$ and $\omega_0 = 20\,000\mathrm{rad/s}$ are presented in Fig. 4. The input power P_{in} is $1\mathrm{W/cm}^2$ and the observation point is at $x = 5\,\mathrm{cm}$. The original signal $g(t)$ is also shown in the figure for reference. It is found that the acoustic wave takes 0.144 ms to propagate from $x = 0$ to $x = 5\,\mathrm{cm}$, which is precisely the value $0.05\,\mathrm{m}/(347\,\mathrm{m/s})$. In Fig. 4, the acoustic signal has the same wave form with the original signal $g(t)$. In addition, the approximate acoustic field agrees well with the exact acoustic field as shown in Fig. 4 which also validates the approximation.

C. Periodic triangle wave signal

Triangle wave signal is a common type of signal which is frequently used in signal processing. A schematic of

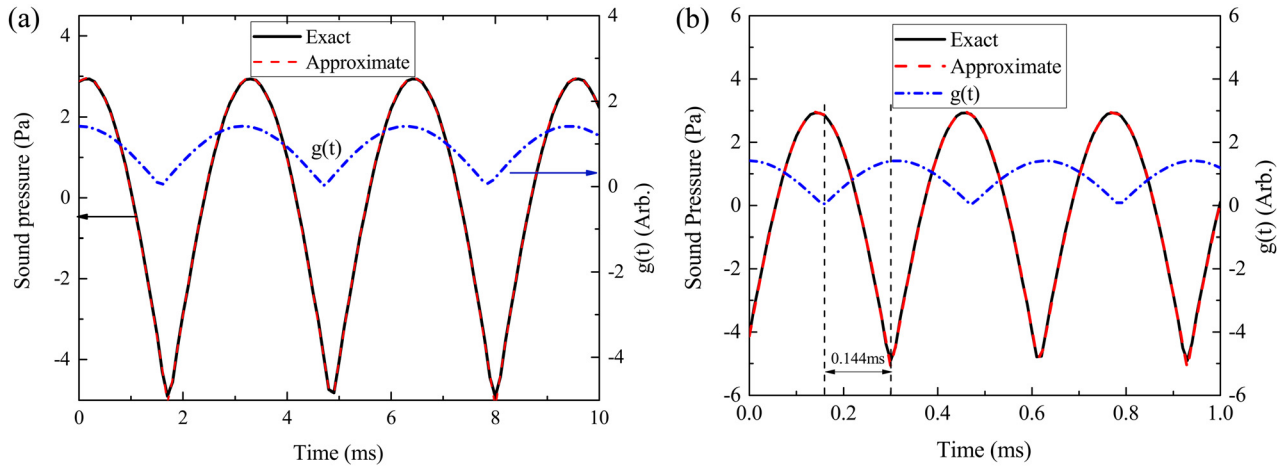

FIG. 4. (Color online) The acoustic pressure response for a square root signal $g(t) = \sqrt{1+\cos(\omega_0 t)}$ at 1 W/cm^2 input power, (a) $\omega_0 = 2000$rad/s, (b) $\omega_0 = 20\ 000$rad/s. The first ten terms ($n = 1-10$) are used to calculate the exact acoustic pressure in (a) and (b).

triangle wave signal with period T is shown in Fig. 5(a). For $-T/2 < t < T/2$, we have $g(t) = (1-2|t|/T)$. The cosine series expression of $g(t)$ can be expressed as

$$g(t) = \frac{1}{2} + \frac{4}{\pi^2}\sum_{n=1}^{\infty}\frac{1}{(2n-1)^2}\cos[(2n-1)\omega_0 t], \tag{34}$$

where $\omega_0 = 2\pi/T$. Applying Fourier transformation to the triangular function $g(t)$ yields

$$G(\omega) = \sqrt{\frac{\pi}{2}}\delta(\omega) + \frac{4}{\pi^2}\sum_{n=1}^{\infty}\sqrt{\frac{\pi}{2}}\frac{1}{(2n-1)^2} \times [\delta(\omega-(2n-1)\omega_0) + \delta(\omega+(2n-1)\omega_0)]. \tag{35}$$

Substituting Eq. (35) into the integral in Eq. (19), the acoustic field becomes

$$P(x,t) = \sum_{n=1}^{\infty}\frac{2}{\pi^2}\frac{1}{(2n-1)^2}\left\{\bar{P}\left(x,(2n-1)\omega_0\right)e^{j(2n-1)\omega_0 t} + \bar{P}\left(x,-(2n-1)\omega_0\right)e^{-j(2n-1)\omega_0 t}\right\}. \tag{36}$$

Because $\bar{P}(x,0) = 0$, it has no contribution to the final acoustic pressure. Hence it is omitted in Eq. (36). Using Eq. (32), the approximate acoustic field can also be directly expressed as

$$P(x,t) = P_{\text{in}}\frac{\gamma-1}{2C_0}\left(\frac{1}{2} - \frac{2}{T}\left|t - \frac{x}{C_0}\right|\right)\left(-\frac{T}{2} < t < \frac{T}{2}\right). \tag{37}$$

The approximate acoustic field beyond the time period (−T/2,T/2) can also be obtained using the same approach.

The exact and approximate acoustic field solutions are compared in Fig. 6. It is found that the wave form of acoustic signal is almost similar to the input signal $g(t)$, i.e., the acoustic signal has recovered the input signal $g(t)$ with a small distortion. For input signal with period T = 1 ms, the approximate solution agrees well with the exact one. While for period T = 0.05 ms, the approximate solution slightly deviates from the exact solution because the input signal spectrum gradually changes from low frequency to high frequency as the period decreases. When the period is further reduced to a critical value, the lowest frequency component exceeds the upper boundary $\text{Min}\{(4\kappa_g{}^2)/(\alpha_g c_s{}^2), C_0{}^2/\alpha_g\}$, then the approximate solution becomes invalid. Therefore, it is concluded that the TA sound signal is able to well recover the input periodic triangle signal at an order of microsecond.

D. Periodic rectangular pulse signal

Rectangular pulse signal is another common type of signal in signal processing. A schematic of a rectangular pulse

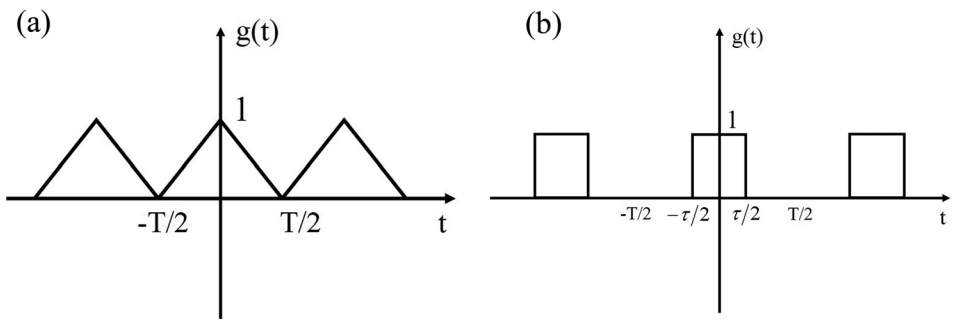

FIG. 5. (a) Triangle wave signal with period T and (b) rectangular wave signal with period T. The pulse width of rectangular wave signal is τ.

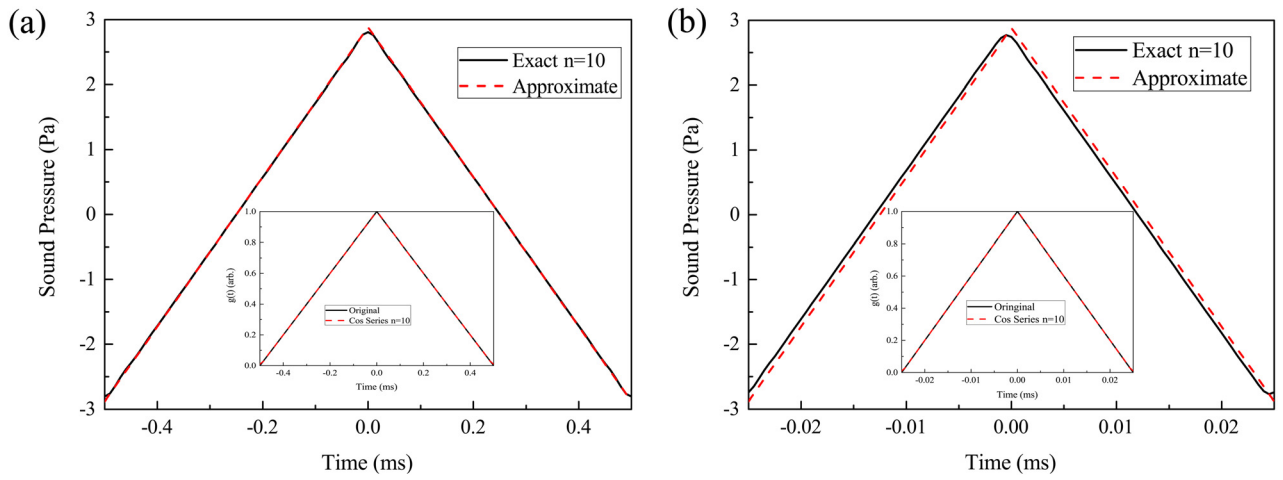

FIG. 6. (Color online) The acoustic pressure response for a periodic triangle signal at 1 W/cm^2 input power. (a) T = 1 ms, (b) T = 0.05 ms. The first 10 terms ($n = 1 - 10$) are used to calculate the exact acoustic pressure in (a) and (b). The figures inserted in (a) and (b) are the signals $g(t)$ with period 1 and 0.1 ms, respectively.

signal with a period T and a pulse width τ is shown in Fig. 5(b). The acoustic field driven by the rectangular pulse signal expressed in terms of a cosine series is

$$g(t) = \frac{\tau}{T} + \frac{4}{T\omega_0}\sum_{n=1}^{\infty}\frac{1}{n}\sin\frac{n\omega_0\tau}{2}\cos(n\omega_0 t), \tag{38}$$

where $\omega_0 = 2\pi/T$. Applying Fourier transformation on Eq. (38) gives

$$G(\omega) = \frac{\tau}{T}\sqrt{2\pi}\delta(\omega) + \frac{4}{T\omega_0}\sum_{n=1}^{\infty}\frac{1}{n}\sqrt{\frac{\pi}{2}}\sin\frac{n\omega_0\tau}{2} \times \left[\delta(\omega - n\omega_0) + \delta(\omega + n\omega_0)\right]. \tag{39}$$

Substituting Eq. (39) into Eq. (19) yields the following acoustic field

$$p(x,t) = \frac{2}{T\omega_0}\sum_{n=1}^{\infty}\frac{1}{n}\sin\frac{n\omega_0\tau}{2} \times \left[\bar{P}(x,n\omega_0)e^{jn\omega_0 t} + \bar{P}(x,-n\omega_0)e^{-jn\omega_0 t}\right]. \tag{40}$$

The approximate acoustic field solution for one period can be easily obtained as

$$P(x,t) = \begin{cases} P_{\text{in}}\dfrac{\gamma-1}{2C_0}\left(1-\dfrac{\tau}{T}\right) & \left(-\dfrac{\tau}{2} < t < \dfrac{\tau}{2}\right) \\ -P_{\text{in}}\dfrac{\tau}{T}\dfrac{\gamma-1}{2C_0} & \left(\dfrac{\tau}{2} < |t| < \dfrac{T}{2}\right). \end{cases} \tag{41}$$

A comparison of the exact and approximate solutions for various periods T and pulse widths τ is shown in Fig. 7. Generally, the approximate solution and the exact solution are consistency. The small fluctuation of the exact solution around the discontinuity points is called the Gibbs effect that cannot be avoided theoretically. As τ/T decreases, the positive acoustic pressure tends to be more dominant as shown in Figs. 7(b) and 7(d) and the acoustic signal resembles a pulse signal. For an amplitude of $g(t)$ that equals to 1 arbitrary unit, the input signal $f(t)$ is the same as $g(t)$. As a result, the acoustic signal recovers the input signal $f(t)$ with a small distortion.

It is well known the harmonic distortion for a TA device is an inherent problem. The common treatment is to superpose a direct current to the signal to eliminate the double-frequency output signal. However, the power consumption is high by using this method. By digitizing the input signal $f(t)$ before applying to the TA device, $f(t)$ becomes a series of pulse signals. Thus the TA device recovers the signal without the need of additional treatment. By using this method, the distortion is small and the power consumption is low. It was experimentally verified by Koshida *et al.* (Koshida *et al.*, 2013). In the experiment, the input analog signal was converted by the density modulation into pulse trains and applied to the TA device. The experiment result showed that the total harmonic distortion was only about 1%. Further numerical analysis indicates that when the period of signal $g(t)$ is less than 0.01 ms, the approximate solution deviates from the exact solution. The cause is similar to that mentioned in the previous subsection. Nevertheless, when the pulse width is sufficiently small, the output acoustic signal can still be a pulse signal.

E. Alternative method for recovery of original signal *f(t)*

In the preceding sections, the main focus is on the response for signal $g(t)$. For $g(t) = f^2(t)$, the acoustic field response is $f^2(t)$ but not the original signal $f(t)$. There are distortions of the acoustic signals with respect to the original signal. The frequently used method to recover the original signal is to do signal amplitude modulation and then superposes onto a direct current. The original signal is converted to $1 + mf(t)$, with m the modulation depth. For $m \ll 2$, we have $g(t) \approx 1 + 2mf(t)$. Neglecting the DC signal in $g(t)$, then the original signal $f(t)$ can be recovered. However, it is obvious that the power consumption is high because most of

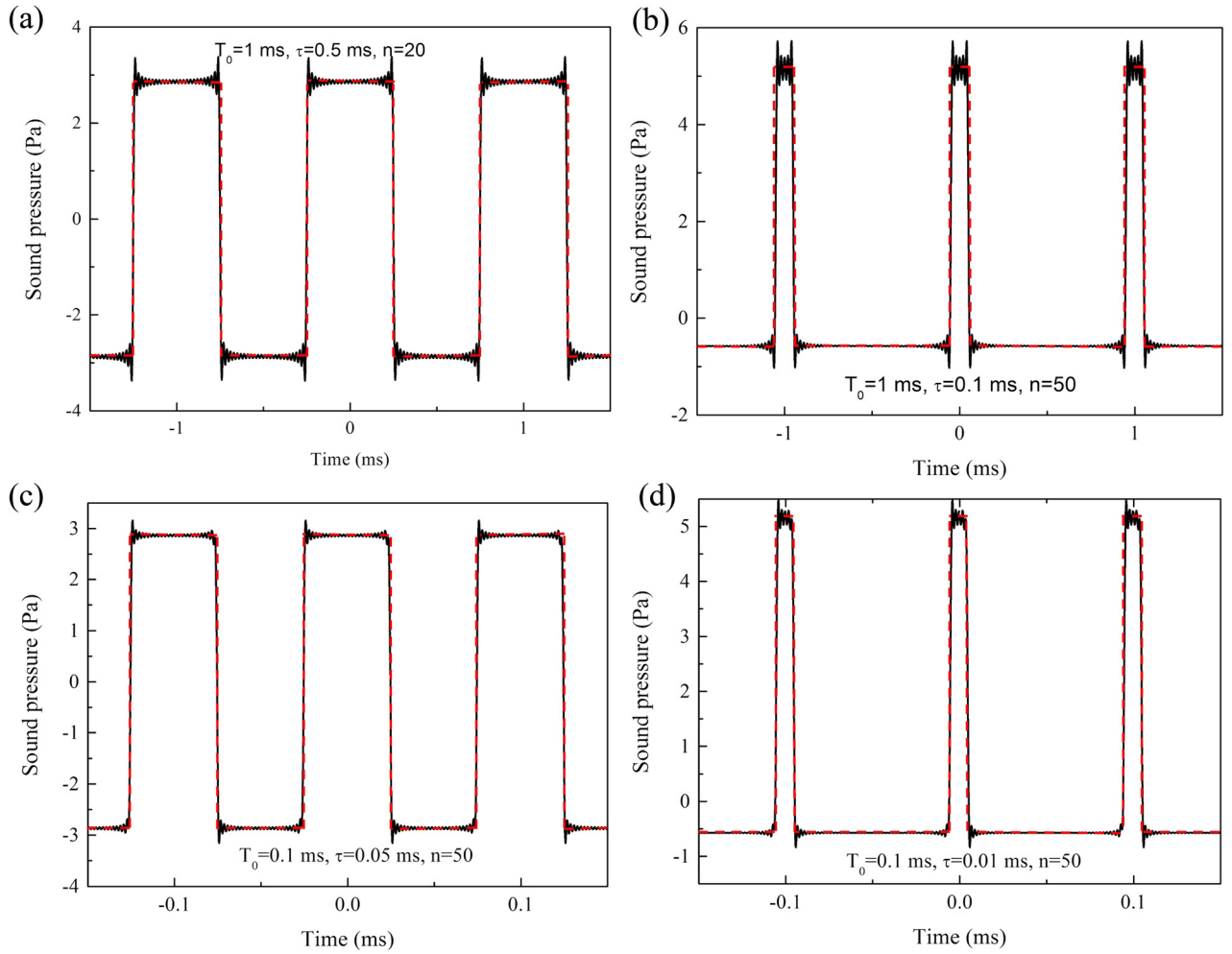

FIG. 7. (Color online) The acoustic pressure response for a periodic rectangular pulse signal at 1 W/cm^2 input power. (a) T = 1 ms, $\tau = 0.5$ ms, (b) T = 1 ms, $\tau = 0.1$ ms, (c) T = 0.1 ms, $\tau = 0.05$ ms, (d) T = 0.1 ms, $\tau = 0.01$ ms. The red dotted line is the approximate solution, the black solid line is the exact solution.

the thermal energy is generated by DC which does not contribute to the acoustic pressure. If the original signal is superposed with a DC and then converted to a square rooting signal, i.e., the original signal $f(t)$ is converted to $\sqrt{I_{\mathrm{DC}} + f(t)}$, where I_{DC} is a DC signal to guarantee $I_{\mathrm{DC}} + f(t)$ be positive. When the processed signal is applied to the TA device, then $g(t) = I_{\mathrm{DC}} + f(t)$, the original signal can thus be recovered. If the superposed DC signal is a constant, it also leads to significant power waste for some types of signals. Therefore, the DC signal should be designed that the minimized value is selected in order to guarantee $I_{\mathrm{DC}} + f(t)$ be positive. For example, for an input signal $f(t) = \cos(\omega_0 t)$, $I_{\mathrm{DC}} = 1$ is selected. For a positive periodic rectangular pulse signal input as shown in Fig. 5(b), $I_{\mathrm{DC}} = 0$ is selected. Following this procedure, it is theoretically possible to have no output acoustic signal distortion while having significantly lower power consumption than other conventional methods. For a positive input signal, theoretically there is no extra power consumption produced. This square rooting processing method is also used in the parametric array design for reproducing audible sound by self-demodulation from ultrasound input signal (Pompei, 2003). However, the conventional mechanically driven sound transducers can only perform well around its resonance frequencies. The square root signal is a broadband signal, in which the bandwidth tends to be infinite. Hence, the parametric array signal emitted from the conventional sound transducers is inevitably distorted. Consider TA transducers exhibit the ability of broadband responses, they are excellent candidates for the design of parametric array source (Pompei, 1999). The details for input signal recovery and its application on the parametric array design will be discussed in future works.

IV. CONCLUSIONS

New analytical and approximate solution for acoustic field response to a broadband input signal applying on a TA device is proposed and both free-standing and NTF-substrate TA devices are investigated. The exact and approximate acoustic pressures for these two kinds of devices are obtained by using Fourier transformation and its inverse. The acoustic pressure response to a single-frequency signal for NTF-substrate and free-standing TA devices are theoretically predicted. The new analytical models are verified by comparing with published experiments and excellent

agreement has been demonstrated. To further confirm the ability of broadband signal response of the TA devices, a square rooting signal is investigated. The approximate and exact acoustic fields show that the TA sound signals do recover the wave form of input signals with small distortions. Two other frequently used signals, the periodic triangle and rectangular pulse signals, are also applied to investigate the acoustic pressure responses. The acoustic signal wave forms for these two cases do reproduce the wave form of the input signals within a limited period range. By analyzing acoustic signal generated by a rectangular pulse signal input, it is concluded that the TA device does reproduce the original signal wave form by digitizing the original signal before applying to the TA device. This conclusion offers an alternative method for the recovery of original signal of TA device with small distortion and low power consumption. Note that the conventional method for recovering the original signals requires DC superposition onto modulated original signal and it results in high energy consumption. Here, a new method to recover the original signal is introduced and the advantage of this new method is its low power consumption and small distortion. To further explore and exploit the ability of broadband responses, some superior and practical applications of TA devices for sound parametric array designs and underwater communication equipment will be reported in future works.

ACKNOWLEDGMENTS

This work was supported by the Early Career Scheme (Project No. PolyU 252026/16E) and General Research Grant (Project No. CityU 11215415) from the Research Grants Council of the Hong Kong Special Administrative Region. Foundation Program of Jiangxi Key Laboratory (20161BCD40010) is also acknowledged.

Aliev, A. E., Gartstein, Y. N., and Baughman, R. H. (**2013**). "Increasing the efficiency of thermoacoustic carbon nanotube sound projectors," Nanotechnology **24**, 235501.

Aliev, A. E., Lima, M. D., Fang, S., and Baughman, R. H. (**2010**). "Underwater sound generation using carbon nanotube projectors," Nano Lett. **10**, 2374–2380.

Aliev, A. E., Mayo, N. K., de Andrade, M. J., Robles, R. O., Fang, S. L., Baughman, R. H., Zhang, M., Chen, Y. S., Lee, J. A., and Kim, S. J. (**2015**). "Alternative nanostructures for thermophones," ACS Nano **9**, 4743–4756.

Aliev, A. E., Perananthan, S., and Ferraris, J. P. (**2016**). "Carbonized electrospun nanofiber sheets for thermophones," ACS Appl. Mater. Interfaces **8**, 31192–31201.

Arnold, H. D., and Crandall, I. B. (**1917**). "The thermophone as a precision source of sound," Phys. Rev. **10**, 22–38.

Beranek, L. L., and Mellow, T. (**2012**). *Acoustics: Sound Fields and Transducers* (Academic, New York).

Chitnis, G., Kim, A., Song, S. H., Jessop, A. M., Bolton, J. S., and Ziaie, B. (**2012**). "A thermophone on porous polymeric substrate," Appl. Phys. Lett. **101**, 021911.

Hu, H., Zhu, T., and Xu, J. (**2010**). "Model for thermoacoustic emission from solids," Appl. Phys. Lett. **96**, 214101.

Koshida, N., Hippo, D., Mori, M., Yanazawa, H., Shinoda, H., and Shimada, T. (**2013**). "Characteristics of thermally induced acoustic emission from nanoporous silicon device under full digital operation," Appl. Phys. Lett. **102**, 123504.

Kozlov, M. E., Haines, C. S., Oh, J. Y., Lima, M. D., and Fang, S. L. (**2009**). "Sound of carbon nanotube assemblies," J. Appl. Phys. **106**, 124311.

Lim, C. W., Tong, L. H., and Li, Y. C. (**2013**). "Theory of suspended carbon nanotube thinfilm as a thermal-acoustic source," J. Sound Vib. **332**, 5451–5461.

Mason, B. J., Chang, S. W., Chen, J. H., Cronin, S. B., and Bushmaker, A. W. (**2015**). "Thermoacoustic transduction in individual suspended carbon nanotubes," ACS Nano **9**, 5372–5376.

Niskanen, A. O., Hassel, J., Tikander, M., Maijala, P., Gronberg, L., and Helisto, P. (**2009**). "Suspended metal wire array as a thermoacoustic sound source," Appl. Phys. Lett. **95**, 163102.

Pompei, F. J. (**1999**). "Beams of sound: A low-distortion airborne parametric array," J. Acoust. Soc. Am. **105**, 1372–1372.

Pompei, F. J. (**2003**). "Sound from Ultrasound: The parametric array as an audible sound source," Ph.D. thesis, Massachusetts Institute of Technology.

Shinoda, H., Nakajima, T., Ueno, K., and Koshida, N. (**1999**). "Thermally induced ultrasonic emission from porous silicon," Nature **400**, 853–855.

Suk, J. W., Kirk, K., Hao, Y. F., Hall, N. A., and Ruoff, R. S. (**2012**). "Thermoacoustic sound generation from monolayer graphene for transparent and flexible sound sources," Adv. Mater. **24**, 6342–6347.

Tian, H., Li, C., Mohammad, M. A., Cui, Y. L., Mi, W. T., Yang, Y., Xie, D., and Ren, T. L. (**2014**). "Graphene earphones: Entertainment for both humans and animals," ACS Nano **8**, 5883–5890.

Tian, H., Ren, T.-L., Xie, D., Wang, Y.-F., Zhou, C.-J., Feng, T.-T., Fu, D., Yang, Y., Peng, P.-G., Wang, L.-G., and Liu, L.-T. (**2011a**). "Graphene-on-paper sound source devices," ACS Nano **5**, 4878–4885.

Tian, H., Xie, D., Yang, Y., Ren, T. L., Lin, Y. X., Chen, Y., Wang, Y. F., Zhou, C. J., Peng, P. G., Wang, L. G., and Liu, L. T. (**2011b**). "Flexible, ultrathin, and transparent sound-emitting devices using silver nanowires film," Appl. Phys. Lett. **99**, 253507.

Tian, H., Xie, D., Yang, Y., Ren, T. L., Wang, Y. F., Zhou, C. J., Peng, P. G., Wang, L. G., and Liu, L. T. (**2012**). "Single-layer graphene sound-emitting devices: Experiments and modeling," Nanoscale **4**, 2272–2277.

Tong, L. H., Lim, C. W., Lai, S. K., and Li, Y. C. (**2015**). "Gap separation effect on thermoacoustic wave generation by heated suspended CNT nano-thinfilm," Appl. Therm. Eng. **86**, 135–142.

Tong, L. H., Lim, C. W., and Li, Y. C. (**2013**). "Gas-filled encapsulated thermal-acoustic transducer," Trans. ASME J. Vib. Acoust. **135**, 051033.

Tong, L. H., Lim, C. W., Zhao, X. S., and Geng, D. X. (**2016**). "Theory and modeling of cylindrical thermo-acoustic transduction," Phys. Lett. A **380**, 2123–2128.

Venkatasubramanian, R. (**2010**). "Applied physics nanothermal trumpets," Nature **463**, 619–619.

Vesterinen, V., Niskanen, A. O., Hassel, J., and Helistö, P. (**2010**). "Fundamental efficiency of nanothermophones: Modeling and experiments," Nano Lett. **10**, 5020–5024.

Wei, Y., Lin, X. Y., Jiang, K. L., Liu, P., Li, Q. Q., and Fan, S. S. (**2013**). "Thermoacoustic chips with carbon nanotube thin yarn arrays," Nano Lett. **13**, 4795–4801.

Xiao, L., Chen, Z., Feng, C., Liu, L., Bai, Z.-Q., Wang, Y., Qian, L., Zhang, Y., Li, Q., Jiang, K., and Fan, S. (**2008**). "Flexible, stretchable, transparent carbon nanotube thin film loudspeakers," Nano Lett. **8**, 4539–4545.

Xiao, L., Liu, P., Liu, L., Li, Q., Feng, Z., Fan, S., and Jiang, K. (**2011**). "High frequency response of carbon nanotube thin film speaker in gases," J. Appl. Phys. **110**, 084311.